ACS Energy LETTERS

http://pubs.acs.org/journal/aelccp

Divergent Synthesis of Bipolar Membranes Combining Strong Interfacial Adhesion and High-Rate Capability

Yi-Lin Kao, Lihaokun Chen, Shannon W. Boettcher, and David Aili*

Cite This: *ACS Energy Lett.* 2024, 9, 2953−2959

Read Online

ACCESS | Metrics & More | Article Recommendations | Supporting Information

ABSTRACT: **Bipolar membranes are emerging as attractive solid electrolytes for water electrolysis, electrochemical CO_2 reduction, and CO_2 capture by base from electrodialysis. The development of these technologies is currently hampered by the resistance of current commercial materials under reversed bias, as well as interfacial incompatibility between the layers that can lead to delamination. This letter reports a divergent route to a nonfluorinated TiO_2-catalyzed bipolar membrane, where the interfacial compatibility is governed by constructing the cation/anion exchange layers from the same backbone chemistry. We show that this BPM design concept has the potential to drastically enhance the adhesion strength at the interfacial junction, without compromising rate capability under bipolar membrane water electrolysis conditions.**

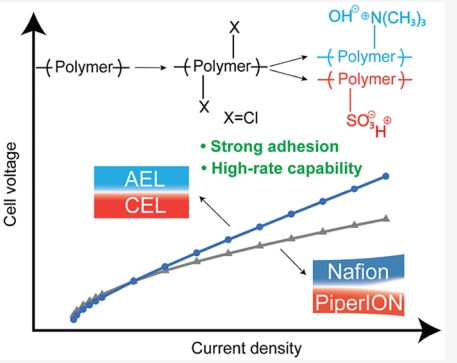

A bipolar membrane (BPM) is a laminate of anion- and cation-exchange ionomer layers that can support water dissociation and ionic separation of H^+ and OH^- ions under the influence of an applied voltage.[1−3] The result is the buildup of a pH gradient across the BPM, which can be used for pH adjustments in various industrial chemical and biochemical processes.[4,5] BPM electrodialysis can also be used for acid/base generation from aqueous salt solutions[6] and further in conjunction with CO_2 capture processes that use pH swings.[7,8] Furthermore, the use of a BPM in water and CO_2 electrolysis cells has been found to effectively mitigate unwanted reactant/product crossover[9,10] and to provide electrochemical environments that contribute to performance gains and to improved utilization of precious metals.[11−15]

One of the main hurdles in the development of electrochemical devices based on BPMs is the high resistance of commercial materials at practical current densities, which mainly originates from the slow water dissociation (WD) reaction at the interface between the anion and cation exchange layers.[16] This has triggered tremendous research efforts spanning from mapping and probing of phenomena that govern water dissociation and ionic separation[17−19] to the design of new BPMs with enhanced water dissociation activity[20−23] and mass transport characteristics.[13,24] The evaluation of different water dissociation catalysts currently points to graphene oxide,[25−27] TiO_2,[23] and SnO_2[28] as good candidates that combine high activity, earth abundancy, and good stability. Remarkably high-rate capability has recently been reported for TiO_2- and SnO_2-catalyzed BPMs with cation exchange layers (CELs) and anion exchange layers (AELs) based on perfluorosulfonic acid (Nafion) and poly(arylene piperidinium) (PiperION), respectively.[18,23,28]

A large majority of the BPMs reported in the literature are based on individual CELs/AELs of vastly different backbone chemistry, which often result in low adhesion strength at the CEL/AEL interface and therefore blistering and delamination during operation.[2] Physical anchoring of the individual layers by entanglement of nanofibers at the interface[20,22,29,30] or covalent interlocking[31,32] has recently been explored to mitigate delamination. Furthermore, many of the reported BPMs are constructed based on perfluorinated CELs, which may be problematic from environmental and sustainability perspectives.[33]

This work addresses these challenges by constructing a BPM based on a single nonfluorinated polymer through divergent functionalization of poly(styrene-*b*-poly(ethylene-*ran*-butylene)-*b*-polystyrene) (SEBS). As shown in Scheme 1, the individual layers were obtained via chloromethylation, followed

Received: April 29, 2024
Revised: May 21, 2024
Accepted: May 22, 2024
Published: May 28, 2024

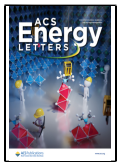

https://doi.org/10.1021/acsenergylett.4c01178
ACS Energy Lett. 2024, 9, 2953−2959

Scheme 1. Divergent Synthetic Route to the Individual Layers of the BPM[a]

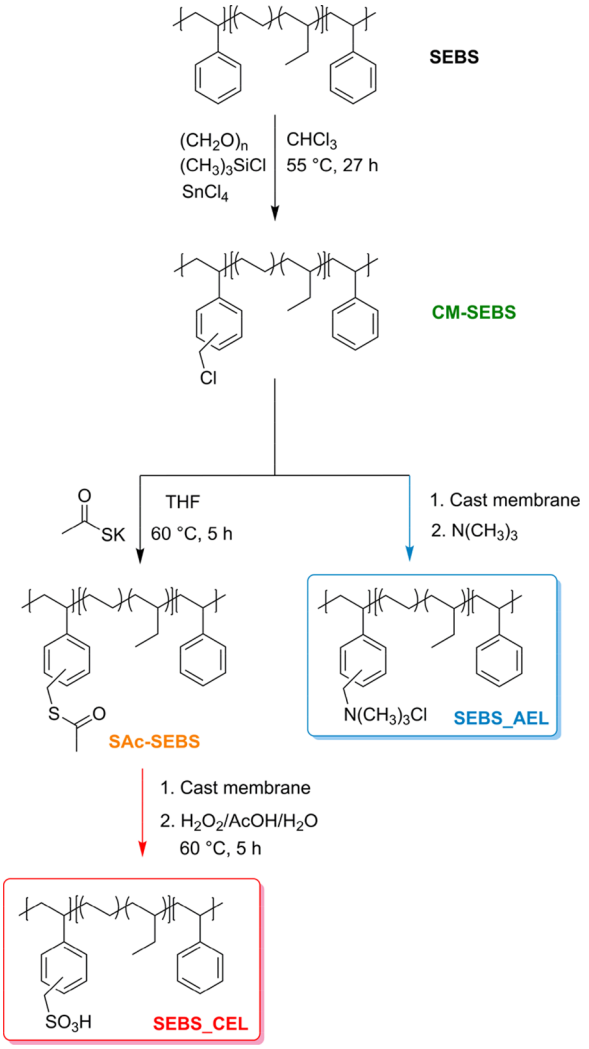

[a]The degree of chloromethylation, calculated from ^{1}H NMR data, was 73% of the styrene unit in the parent SEBS. Chloromethylated SEBS (CM-SEBS) underwent the divergent route to form the quaternary ammonium SEBS as SEBS_AEL and the sulfonated SEBS as SEBS_CEL (see section S1.2 for details).

by a heterogeneous Menshutkin reaction for the AEL[34] or substitution with thioacetate followed by heterogeneous oxidation to the corresponding sulfonic acid for the CEL.[35] The precursor polymer films were cast to a thickness of 50−60 μm, and the final synthetic steps were carried out heterogeneously due to the insolubility of the sulfonated SEBS (SEBS_CEL) and quaternary ammonium functionalized SEBS (SEBS_AEL). The ^{1}H NMR and FTIR spectra of the intermediates and products are shown in Figures S1 and S2, respectively. Table 1 summarizes the ion-exchange capacity (IEC), water uptake (WU), swelling in thickness (SW_T), and in-plane ionic conductivity of the individual SEBS_AEL and SEBS_CEL. Both layers were derived from the same polymer precursor, and the IECs were therefore similar. However, the SEBS_AEL showed a considerably higher WU than the SEBS_CEL.

The SEBS-derived BPMs (SEBS_BPM) were thereafter prepared by spin coating an ink of TiO_2 dispersed in a H_2O/IPA mixture onto the SEBS_CEL (in H^+ form), followed by lamination of the SEBS_AEL (in OH^- form) without pressing. Figure 1a,b shows SEM top-down and cross-section images of the SEBS_BPM prepared from an ink containing 0.5% TiO_2, respectively. The thickness of the TiO_2 interfacial layer was estimated to be 120 nm, and the top-down morphology image shows a nearly complete TiO_2 coverage of the SEBS_CEL surface. Different loadings of TiO_2 were achieved by spin coating with an ink dispersion of different TiO_2 concentrations in a 1:1 weight ratio of a H_2O/IPA mixture onto the SEBS_CEL surface. The specific mass loading of TiO_2 could not be determined reliably by conventional gravimetric methods due to the small masses and the response to humidity changes. Therefore, the obtained BPMs are denoted as SEBS-*XX*%, where *XX* is the TiO_2 content of the spin coating ink, in line with procedures described in the literature.[18] An estimation of the corresponding TiO_2 mass loadings based on SEM top-down images using *ImageJ* is shown in section S1.5 in the Supporting Information. Note that 0.2%, 0.5%, and 1% were used as the concentrations prepared, while samples with 2% and 4% were prepared by 1% ink spin coated two and four times, respectively. Thus, the notations 2% and 4% do not correspond to the specific ink concentrations but refer to the spin-coating of 2 and 4 layers of the 1% ink, respectively. The morphology of the TiO_2-coated SEBS_CEL was examined via top-down SEM imaging, with 0.2% showing the lowest surface coverage of TiO_2, while 4% had the densest surface coverage (Figure S5).

In addition to having a straightforward synthetic route for the BPM development, our hypothesis was that the identical backbone chemistry would lead to improved junction adhesion, in particular for BPMs fabricated from direct lamination. To test this hypothesis, the interfacial layer compatibility of the SEBS_BPM was assessed by recording the adhesion force between SEBS_CEL and SEBS_AEL with and without TiO_2 at the interface via a T-peel strength test (Figure 1c). The junction adhesion force of SEBS_BPM was compared with the baseline 2D junction BPMs derived from

Table 1. Ion Exchange Capacity, Conductivity, Water Uptake, and Swelling of the Individual SEBS_CEL and SEBS_AEL with Thicknesses of 86 ± 3 and 66 ± 4 μm, Respectively[a]

	IEC (meq/g)	conductivity (mS/cm)[b]	WU (%)	SW_T (%)	λ (H_2O per $-SO_3^-$ or $-N(CH_3)_3^+$)
SEBS_CEL	1.51 ± 0.09	46 (25 °C)	39.0 ± 4 (22 °C[c])	22.1 ± 7.2 (22 °C[c])	14.4 ± 1.3 (22 °C[c])
		71 (55 °C)	48.1 ± 2.4 (55 °C)	28.4 ± 8.0 (55 °C)	17.8 ± 1.5 (55 °C)
SEBS_AEL	1.46 ± 0.07	41 (25 °C)	84.4 ± 16 (22 °C[c])	8.0 ± 2.0 (22 °C[c])	32.4 ± 7.6 (22 °C[c])
		65 (55 °C)	100 ± 10 (55 °C)	17.7 ± 7.3 (55 °C)	38.3 ± 5.5 (55 °C)

[a]The conductivity data are the average of two samples, while the other data represent the average and standard deviation for three samples. [b]CEL in H^+ form and AEL in OH^- form. The true OH^- conductivity was determined as described in the literature;[36] see Figure S4. [c]Measured at room temperature: ~22 ± 2 °C.

https://doi.org/10.1021/acsenergylett.4c01178
ACS Energy Lett. 2024, 9, 2953−2959

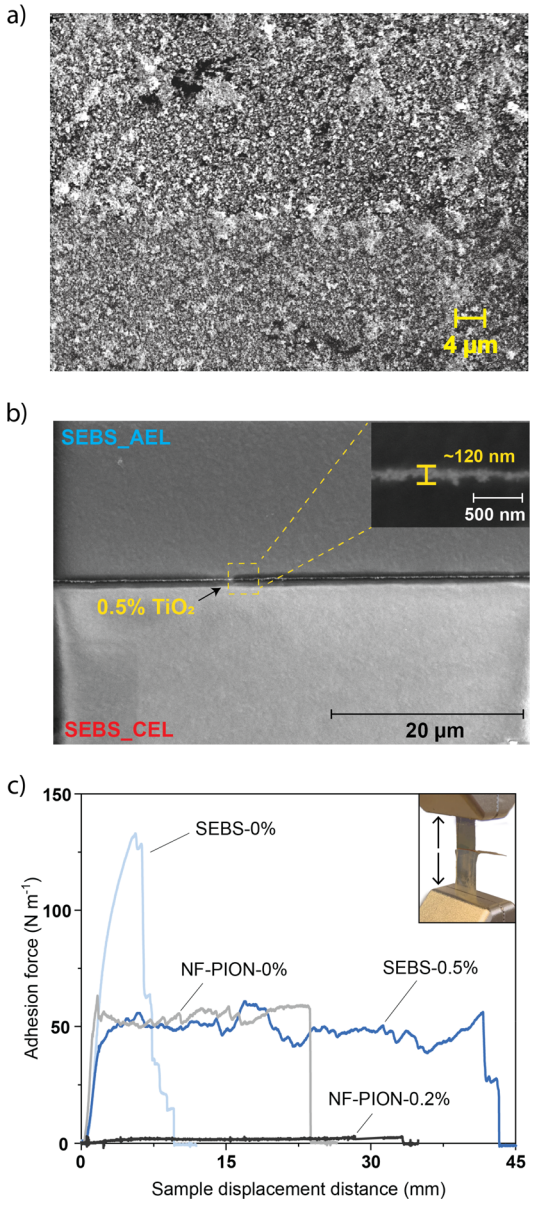

Figure 1. (a) Top-down SEM image of SEBS_CEL spin coated with an ink containing 0.5% TiO_2. (b) Cross-sectional SEM of SEBS-0.5% with a thickness of the interfacial layer of ca. 120 nm. (c) Adhesion force as a function of sample displacement from a 180° T-peel strength for SEBS and NF-PION with and without water dissociation catalyst. The inset shows a photograph of SEBS-0.5% during the T-peel test.

Nafion and PiperION (NF-PION).[23] For the pristine SEBS_CEL and SEBS_AEL laminate without TiO_2 between the layers, the test resulted in deformation of the bulk materials rather than delamination, indicating high interfacial compatibility and strong adhesion energy. A strong adhesion can be observed upon contact of SEBS_CEL and SEBS_AEL, as shown in a video in the Supporting Information. The adhesion force of a NF-PION laminate without water dissociation catalyst was 50 N m^{-1}. After application of TiO_2 from an ink with a concentration of 0.2%, which has been identified as the optimal composition for the NF-PION system,[23] the adhesion force of the NF-PION laminate was only around 5 N m^{-1}, while the adhesion force of the SEBS_ BPM was about 1 order of magnitude higher.

After comprehensive chemical and physical characterizations of the SEBS_CEL and SEBS_AEL, the BPM prepared from an ink containing 0.5% TiO_2 (i.e., SEBS-0.5%) was examined and compared with a commercial BPM (FumaSep FBM) in a four-electrode H-cell using neutral electrolyte of 0.5 M aqueous KNO_3. The polarization curves (j–V curve) at 25 and 55 °C are shown in Figure 2. H-cell measurements have been

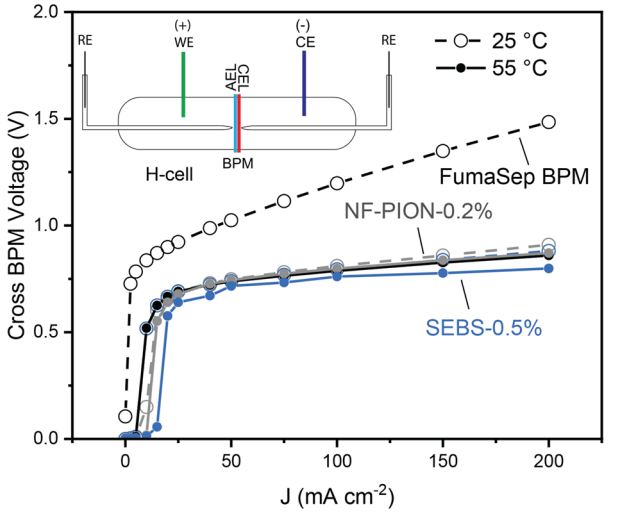

Figure 2. BPM polarization curves recorded in a four-electrode H-cell at 25 and 55 °C using 0.5 M aqueous KNO_3 as electrolyte. The voltage across the BPM was estimated from the voltage measured between two Ag/AgCl reference electrodes placed in Luggin capillaries near each side of the BPM as a function of applied current densities. V_{onset} values at 25 °C are 0.85, 0.69, and 0.68 V for FumaSep BPM, SEBS-0.5%, and NF-PION-0.2%, respectively.

extensively used as a first-line evaluation tool to assess the water dissociation performance before implementing the fabricated BPM in various applications.[16,29,30,37,38] The j–V curve of a BPM with neutral electrolyte in the H-cell characterizes the onset of the water dissociation reaction when the cross membrane voltage (not iR corrected) exceeds the thermodynamic potential of 0.83 V at standard conditions (protons in the CEL and hydroxide in the AEL are each at unit activity) across the BPM interface.[3,5] As shown in Figure S6, the onset potential (V_{onset}) was determined by the intersection of two tangent lines of the polarization curve before and after the evident start of the water dissociation reaction.[21,29] The onset potential of 0.85 V determined for the commercial FumaSep BPM at 25 °C is in good agreement with previous studies under similar conditions (Table S2).[21,27,29,30] V_{onset} = 0.69 V of SEBS-0.5% at 25 °C is close to those of various customized BPMs reported in the literature, as summarized in Table S2. The elevated temperature resulted in lowered cross-membrane voltages, with a more significant impact on the commercial FumaSep BPM. The temperature dependence of the SEBS-0.5% was similar to that of the NF-PION-0.2%, which is discussed in more detail elsewhere.[18] At low cross BPM voltages (before the V_{onset}), 2D junction BPMs show slightly higher currents contributed from the co-ion crossover than the FumaSep BPM.

Following the initial H-cell tests of SEBS-0.5%, the impact of TiO_2 loading on polarization performance was thereafter characterized in a membrane electrode assembly (MEA) water electrolyzer fed by pure water at 55 °C (Figure 3a). The cell

https://doi.org/10.1021/acsenergylett.4c01178
ACS Energy Lett. 2024, 9, 2953−2959

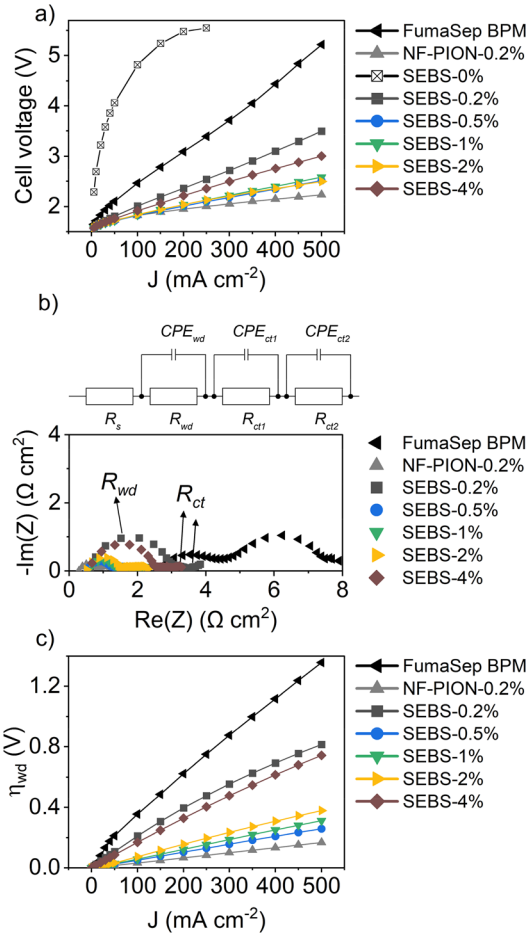

Figure 3. (a) Water electrolysis j−V curves in MEA at 55 °C fabricated with the SEBS-derived BPM with different TiO_2 loadings, using Co_3O_4 on stainless steel for the anode and Pt black on carbon for the cathode. (b) Nyquist plots of the SEBS-derived BPM with different TiO_2 loadings at 100 mA cm^{-2}. The semicircle at high frequency is related to R_{wd} while the semicircles at low frequency are associated to R_{ct}. R_{ct} is the sum of R_{ct1} + R_{ct2}. The equivalent circuit is used to fit the EIS data, and the fitting results are shown in Figure S9 (c) η_{wd} values of the SEBS_BPM with different TiO_2 loadings extracted from the EIS data.

voltages at 500 mA cm^{-2} for SEBS-0.2%, SEBS-0.5%, SEBS-1%, SEBS-2%, and SEBS-4% were 3.5, 2.5, 2.6, 2.5, and 3.0 V, respectively. This trend is consistent with the loading dependence on BPM's performance previously reported for NF-PION,[23] but with an optimum at slightly higher TiO_2 loading for the SEBS-derived analogue (SEBS-0.5%). As shown in Figure S5, SEBS-0.2% presented a relatively low TiO_2 coverage, while the coverage of SEBS-0.5% was nearly complete. The lower performance of SEBS-1%, SEBS-2%, and SEBS-4% could likely be explained by a larger thickness of the junction, which lowers the electric field across the junction and results in increasing ionic resistance for H^+ and OH^- ions migrating from the junction toward the SEBS_CEL and SEBS_AEL, respectively.[39]

In contrast to the cell equipped with the FumaSep membrane, the cells with the SEBS-derived BPM showed no apparent signs of mass transport limitations at >300 mA cm^{-2}. Mass transport of water may become critical during operation at high current densities,[13,24] and the high WU of the SEBS_AEL could potentially play an important role in the water management of this electrolyte system.

Since the MEA electrolyzer cell voltage contains contributions from the anode and cathode, the water dissociation overpotential (η_{wd}) is a more appropriate performance indicator of the BPM alone. As previously reported,[23] η_{wd} can be isolated via electrochemical impedance spectroscopy (EIS) by identifying the water dissociation resistance (R_{wd}) as associated with the high-frequency impedance arc from the total-cell impedance in a Nyquist plot (Figure 3b). The resistance contributions were acquired by fitting EIS results to the equivalent circuit shown in Figure 3b. The high-frequency semicircle represents R_{wd}, and the low-frequency semicircles represent the charge-transfer resistance (R_{ct}), where R_{ct} is the sum of the charge transfer resistances of both electrodes (R_{ct1} and R_{ct2}). According to eq 1, integrating R_{wd} as a function of current density allows us to extract η_{wd}, which is shown in Figure 3c.

$$\eta_{wd} = \int_0^j R_{wd}(j)\, dj \tag{1}$$

The trend of η_{wd} with different TiO_2 loadings corresponds to the trend of the cell voltage, with 0.5% TiO_2 possessing the lowest η_{wd} of 0.26 V at 500 mA cm^{-2} among all loadings. The best-performing SEBS-0.5% not only outperformed the commercial BPM but also showed performance comparable to that of the NF-PION-derived BPM in an MEA water electrolyzer equipped with identical electrodes and operated under similar conditions. We note that the commercial FumaSep BPM includes an embedded reinforcement material in the membrane, which may contribute additional resistance, especially in the MEA measurements.

Figure 4 shows the R_s, R_{wd}, and R_{ct} values of NF-PION and the SEBS-0.5% at various current densities. The EIS fitting results agree with results from Chen et al.,[23] where R_s and R_{wd} remain nearly constant and R_{ct} changes across current densities. Table 2 summarizes the resistance contributions in the MEA water electrolyzer at 30 and 450 mA cm^{-2}, which indicate that the better cell performance of the cell equipped with NF-PION is due to lower Ohmic resistance (R_s) and R_{wd}. Although electrode conditions for the redox reactions were kept identical, the different membrane−electrode interfaces may be the reason for unexpected deviations on R_{ct} of both BPMs. To keep the conditions consistent with previous work, Nafion and PiperION ionomer were used for the cathode and anode fabrication, respectively, which could contribute to incompatibility between electrodes and the BPM. To further analyze the performance difference, the expected area-specific resistances originating from the CEL and AEL was calculated from the specific conductivity data for the individual layers assuming isotropic conductivity behavior and were found to be 0.27 and 0.11 Ω cm^2 at 55 °C for the SEBS_BPM and NF-PION, respectively. These values correspond to the higher R_s and R_{wd} of the SEBS_BPM from the EIS analysis, indicating the overall performance difference is a result of the conductivity differences of the membrane constituents and not specific to the BPM junction where water dissociation occurs.

The stability of SEBS-0.5% was measured in a MEA electrolyzer operating with a pure-water feed at 500 mA cm^{-2} at 55 °C. Polarization curves and impedance data at current densities of 500, 100, 50, and 30 mA cm^{-2} were collected every 3 h at 500 mA cm^{-2}. The polarization curves

https://doi.org/10.1021/acsenergylett.4c01178
ACS Energy Lett. 2024, 9, 2953−2959

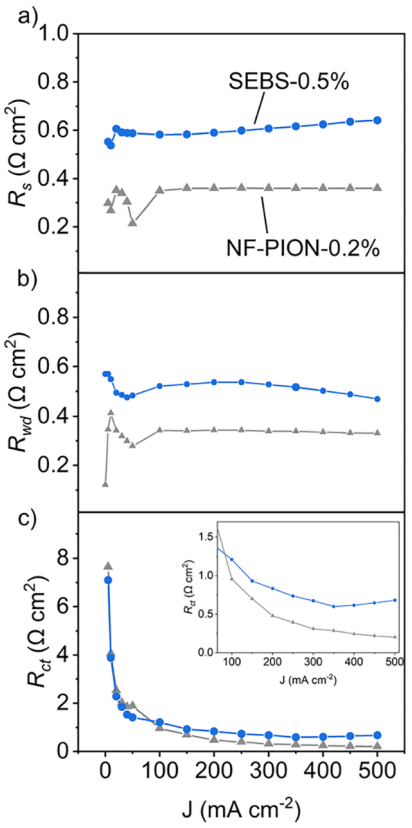

Figure 4. Resistance contributions from R_s (a), R_{wd} (b), and R_{ct} (c) of the SEBS-0.5% and NF-PION-0.2% at various current densities extracted from EIS analysis of BPMs in an MEA water electrolyzer. The inset is a zoom-in at higher current densities.

Table 2. Comparison of Resistance Contributions in the MEA Water Electrolyzer at 30/450 mA cm^{-2}

BPM type	R_s (Ω cm^2)	R_{wd} (Ω cm^2)	R_{ct} (Ω cm^2)
NF-PION-0.2%	0.33/0.36	0.32/0.33	2.03/0.22
SEBS-0.5%	0.59/0.64	0.49/0.48	1.84/0.65

and time evolution of cell voltage are shown in Figure 5a,b, respectively. After the initial characterization cycle to collect the j−V curve, the cell ran for 60 h with a degradation rate of 26 mV h^{-1} in the first 15 h and 7.5 mV h^{-1} after 36 h. After electrolysis testing, the GDEs were strongly adhering to SEBS-0.5% and could not be delaminated. For comparison, the NF-PION-0.2% showed a voltage increase of 15 mV h^{-1} during the first 18 h and 6 mV h^{-1} during the following 18 h,[23] while a rapid degradation in voltage efficiency of the FumaSep BPM was observed within 3 h. The faster voltage increase of the SEBS-0.5% in the beginning of the test may be due to degradation of the AEL, which was equipped with cationic headgroups in benzylic positions that are known to be relatively unstable.[40,41] Ionomer oxidation within the anode may also contribute to the voltage increase,[42] as the cell is operated in pure water without supporting electrolyte to facilitate ionic contact at the BPM−electrode interface. The impedance data also show evidence of degradation over the 60 h test (Figure S10). The increasing R_{wd} values at both low and high current densities indicate degradation of the BPM junction, which confirms the aforementioned degradation of the SEBS_AEL. Although R_{ct} remains stable at the low current densities, it is worth noting that the long-term operation can still suffer from oxidative instability of the anode ionomer.[42] It should be noted that the low-frequency EIS data at 500 mA cm^{-2} is noisy, which results in unreliable fitting values of R_{ct} (Figure S10d). This may be related to degradation of the electrodes at high current densities. Although ex situ studies have shown that the SEBS_AEL shows relatively good stability in 1 M KOH at 60 °C during 30 days,[43] substitution of the cationic head groups with more stable chemistries in combination with the introduction of alkyl spacers to circumvent common degradation pathways will in any case be expected to improve the operating lifetime, perhaps in combination with a protective barrier layer between catalysts and ionomer to mitigate anode degradation.[44]

In summary, this study presents a divergent synthesis route for preparing a BPM from the same polymer backbone structure. The identical polymer backbone matrix with different functional groups was prepared from the same precursor through one-step chloromethylation on the aromatic unit of the backbone structure. The CEL and AEL of a BPM derived from the same precursor ensures the identical backbone structure, which may provide an advantage toward compatibility of the two membrane layers. The elastomeric nature of SEBS and excellent adhesion enabled construction of simple 2D junction morphologies with high-rate capability through direct lamination of the two layers. In an MEA water electrolyzer, the SEBS-derived BPM not only outperformed the commercial FumaSep BPM but also showed performance

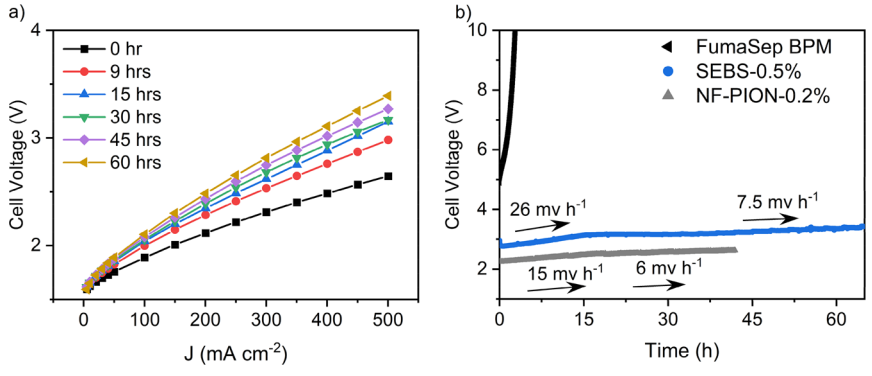

Figure 5. (a) Polarization curves of SEBS-0.5% at different points of operation. (b) Voltage evolution of a MEA water electrolyzer equipped with FumaSep BPM, SEBS-0.5%, and NF-PION-0.2%[23] at 500 mA cm^{-2} at 55 °C (stability test started after the initial current cycle and EIS measurements).

https://doi.org/10.1021/acsenergylett.4c01178
ACS Energy Lett. 2024, 9, 2953−2959

comparable to the best-performing BPM reported in the literature so far. While there is room for improvement in terms of polarization behavior and performance stability through continued optimization of polymer chemistries and junction composition, this work describes a new BPM design concept with the potential to materialize into a new class of nonfluorinated and high-performing BPM for electrochemical devices.

■ ASSOCIATED CONTENT

Supporting Information

The Supporting Information is available free of charge at https://pubs.acs.org/doi/10.1021/acsenergylett.4c01178.

Experimental details, ^{1}H NMR and FTIR data of polymers, illustration showing BPM fabrication process and adhesion between the layers, conductivity data, top-down SEM micrographs after TiO_2 coating, reverse/forward bias cycling, determination of water dissociation onset potential, and electrochemical data for the water electrolysis tests (PDF)

Video showing BPM fabrication process and adhesion between the layers (MP4)

■ AUTHOR INFORMATION

Corresponding Author

David Aili − *Department of Energy Conversion and Storage, Technical University of Denmark, 2800 Lyngby, Denmark;* orcid.org/0000-0002-3510-135X; Email: larda@dtu.dk

Authors

Yi-Lin Kao − *Department of Energy Conversion and Storage, Technical University of Denmark, 2800 Lyngby, Denmark;* orcid.org/0009-0002-1803-456X

Lihaokun Chen − *Department of Chemistry and Biochemistry and the Oregon Center for Electrochemistry, University of Oregon, Eugene, Oregon 97403, United States; Department of Chemical & Biomolecular Engineering and Department of Chemistry, University of California, Berkeley, California 94720, United States; Energy Storage and Distributed Resources Division, Lawrence Berkeley National Laboratory, Berkeley, California 94720, United States*

Shannon W. Boettcher − *Department of Chemistry and Biochemistry and the Oregon Center for Electrochemistry, University of Oregon, Eugene, Oregon 97403, United States; Department of Chemical & Biomolecular Engineering and Department of Chemistry, University of California, Berkeley, California 94720, United States; Energy Storage and Distributed Resources Division, Lawrence Berkeley National Laboratory, Berkeley, California 94720, United States*

Complete contact information is available at: https://pubs.acs.org/10.1021/acsenergylett.4c01178

Notes

The authors declare no competing financial interest.

■ ACKNOWLEDGMENTS

This work was financially supported by Independent Research Fund Denmark (BICON, 0217-00074B). L.C. and S.W.B. acknowledge support from U.S. Office of Naval Research, grants N00014-20-1-2517 and N00014-23-1-2820. Dmytro Serhiichuk, Yifan Xia, and Cenxi Li are thanked for their help during the membrane development phase. Olivia Traenkle and James Mitchell are thanked for advice and practical training associated with the measurement of BPM adhesion.

■ REFERENCES

(1) Oener, S. Z.; Ardo, S.; Boettcher, S. W. Ionic Processes in Water Electrolysis: The Role of Ion-Selective Membranes. *ACS Energy Lett.* **2017**, *2* (11), 2625−2634.

(2) Blommaert, M. A.; Aili, D.; Tufa, R. A.; Li, Q.; Smith, W. A.; Vermaas, D. A. Insights and Challenges for Applying Bipolar Membranes in Advanced Electrochemical Energy Systems. *ACS Energy Lett.* **2021**, *6* (7), 2539−2548.

(3) Tufa, R. A.; Blommaert, M. A.; Chanda, D.; Li, Q.; Vermaas, D. A.; Aili, D. Bipolar Membrane and Interface Materials for Electrochemical Energy Systems. *ACS Appl. Energy Mater.* **2021**, *4* (8), 7419−7439.

(4) Giesbrecht, P. K.; Freund, M. S. Recent Advances in Bipolar Membrane Design and Applications. *Chem. Mater.* **2020**, *32* (19), 8060−8090.

(5) Pärnamäe, R.; Mareev, S.; Nikonenko, V.; Melnikov, S.; Sheldeshov, N.; Zabolotskii, V.; Hamelers, H. V. M.; Tedesco, M. Bipolar Membranes: A Review on Principles, Latest Developments, and Applications. *J. Membr. Sci.* **2021**, *617*, No. 118538.

(6) Davis, J. R.; Chen, Y.; Baygents, J. C.; Farrell, J. Production of Acids and Bases for Ion Exchange Regeneration from Dilute Salt Solutions Using Bipolar Membrane Electrodialysis. *ACS Sustain Chem. Eng.* **2015**, *3* (9), 2337−2342.

(7) Sabatino, F.; Mehta, M.; Grimm, A.; Gazzani, M.; Gallucci, F.; Kramer, G. J.; Van Sint Annaland, M. Evaluation of a Direct Air Capture Process Combining Wet Scrubbing and Bipolar Membrane Electrodialysis. *Ind. Eng. Chem. Res.* **2020**, *59* (15), 7007−7020.

(8) Sharifian, R.; Boer, L.; Wagterveld, R. M.; Vermaas, D. A. Oceanic Carbon Capture through Electrochemically Induced in Situ Carbonate Mineralization Using Bipolar Membrane. *Chem. Eng. J.* **2022**, *438*, No. 135326.

(9) Ma, M.; Kim, S.; Chorkendorff, I.; Seger, B. Role of Ion-Selective Membranes in the Carbon Balance for CO_2 Electroreduction via Gas Diffusion Electrode Reactor Designs. *Chem. Sci.* **2020**, *11* (33), 8854−8861.

(10) Xie, K.; Miao, R. K.; Ozden, A.; Liu, S.; Chen, Z.; Dinh, C.-T.; Huang, J. E.; Xu, Q.; Gabardo, C. M.; Lee, G.; Edwards, J. P.; O'Brien, C. P.; Boettcher, S. W.; Sinton, D.; Sargent, E. H. Bipolar Membrane Electrolyzers Enable High Single-Pass CO_2 Electroreduction to Multicarbon Products. *Nat. Commun.* **2022**, *13*, 3609.

(11) Li, Y. C.; Zhou, D.; Yan, Z.; Gonçalves, R. H.; Salvatore, D. A.; Berlinguette, C. P.; Mallouk, T. E. Electrolysis of CO_2 to Syngas in Bipolar Membrane-Based Electrochemical Cells. *ACS Energy Lett.* **2016**, *1* (6), 1149−1153.

(12) Vermaas, D. A.; Smith, W. A. Synergistic Electrochemical CO_2 Reduction and Water Oxidation with a Bipolar Membrane. *ACS Energy Lett.* **2016**, *1* (6), 1143−1148.

(13) Mayerhöfer, B.; McLaughlin, D.; Böhm, T.; Hegelheimer, M.; Seeberger, D.; Thiele, S. Bipolar Membrane Electrode Assemblies for Water Electrolysis. *ACS Appl. Energy Mater.* **2020**, *3* (10), 9635−9644.

(14) Yan, Z.; Hitt, J. L.; Zeng, Z.; Hickner, M. A.; Mallouk, T. E. Improving the Efficiency of CO_2 Electrolysis by Using a Bipolar Membrane with a Weak-Acid Cation Exchange Layer. *Nat. Chem.* **2021**, *13* (1), 33−40.

(15) Bui, J. C.; Lees, E. W.; Marin, D. H.; Stovall, T. N.; Chen, L.; Kusoglu, A.; Nielander, A. C.; Jaramillo, T. F.; Boettcher, S. W.; Bell, A. T.; Weber, A. Z. Multi-Scale Physics of Bipolar Membranes in Electrochemical Processes. *Nat. Chem. Eng.* **2024**, *1* (1), 45−60.

(16) Blommaert, M. A.; Vermaas, D. A.; Izelaar, B.; In'T Veen, B.; Smith, W. A. Electrochemical Impedance Spectroscopy as a Performance Indicator of Water Dissociation in Bipolar Membranes. *J. Mater. Chem. A* **2019**, *7* (32), 19060−19069.

(17) Oener, S. Z.; Foster, M. J.; Boettcher, S. W. Accelerating Water Dissociation in Bipolar Membranes and for Electrocatalysis. *Science* **2020**, *369* (6507), 1099−1103.

(18) Chen, L.; Xu, Q.; Boettcher, S. W. Kinetics and Mechanism of Heterogeneous Voltage-Driven Water-Dissociation Catalysis. *Joule* **2023**, *7* (8), 1867−1886.
(19) Yan, Z.; Zhu, L.; Li, Y. C.; Wycisk, R. J.; Pintauro, P. N.; Hickner, M. A.; Mallouk, T. E. The Balance of Electric Field and Interfacial Catalysis in Promoting Water Dissociation in Bipolar Membranes. *Energy Environ. Sci.* **2018**, *11* (8), 2235−2245.
(20) Shen, C.; Wycisk, R.; Pintauro, P. N. High Performance Electrospun Bipolar Membrane with a 3D Junction. *Energy Environ. Sci.* **2017**, *10* (6), 1435−1442.
(21) Kole, S.; Venugopalan, G.; Bhattacharya, D.; Zhang, L.; Cheng, J.; Pivovar, B.; Arges, C. G. Bipolar Membrane Polarization Behavior with Systematically Varied Interfacial Areas in the Junction Region. *J. Mater. Chem. A* **2021**, *9* (4), 2223−2238.
(22) Al-Dhubhani, E.; Swart, H.; Borneman, Z.; Nijmeijer, K.; Tedesco, M.; Post, J. W.; Saakes, M. Entanglement-Enhanced Water Dissociation in Bipolar Membranes with 3D Electrospun Junction and Polymeric Catalyst. *ACS Appl. Energy Mater.* **2021**, *4* (4), 3724−3736.
(23) Chen, L.; Xu, Q.; Oener, S. Z.; Fabrizio, K.; Boettcher, S. W. Design Principles for Water Dissociation Catalysts in High-Performance Bipolar Membranes. *Nat. Commun.* **2022**, *13*, 3846.
(24) Oener, S. Z.; Twight, L. P.; Lindquist, G. A.; Boettcher, S. W. Thin Cation-Exchange Layers Enable High-Current-Density Bipolar Membrane Electrolyzers via Improved Water Transport. *ACS Energy Lett.* **2021**, *6* (1), 1−8.
(25) Chen, Y.; Wrubel, J. A.; Klein, W. E.; Kabir, S.; Smith, W. A.; Neyerlin, K. C.; Deutsch, T. G. High-Performance Bipolar Membrane Development for Improved Water Dissociation. *ACS Appl. Polym. Mater.* **2020**, *2* (11), 4559−4569.
(26) Wang, H.; Ding, F.; Jin, G.; Li, C.; Meng, H. Ultra-Thin Graphene Oxide Intermediate Layer for Bipolar Membranes Using Atomizing Spray Assembly. *Colloids Surf. A Physicochem Eng. Asp* **2017**, *520*, 114−120.
(27) McDonald, M. B.; Freund, M. S. Graphene Oxide as a Water Dissociation Catalyst in the Bipolar Membrane Interfacial Layer. *ACS Appl. Mater. Interfaces* **2014**, *6* (16), 13790−13797.
(28) Boettcher, S.; Sasmal, S.; Lihaokun, C.; Sarma, P.; Traenkle, O.; Simons, C.; Wells, K.; Spontak, R. Water-Dissociation Catalysis Near the Reversible Limit in Bipolar Membrane Electrolyzers. *ResearchSquare* 2023. DOI: 10.21203/rs.3.rs-3447094/v1
(29) Powers, D.; Mondal, A. N.; Yang, Z.; Wycisk, R.; Kreidler, E.; Pintauro, P. N. Freestanding Bipolar Membranes with an Electrospun Junction for High Current Density Water Splitting. *ACS Appl. Mater. Interfaces* **2022**, *14* (31), 36092−36104.
(30) Hohenadel, A.; Powers, D.; Wycisk, R.; Adamski, M.; Pintauro, P.; Holdcroft, S. Electrochemical Characterization of Hydrocarbon Bipolar Membranes with Varying Junction Morphology. *ACS Appl. Energy Mater.* **2019**, *2* (9), 6817−6824.
(31) Xu, Z.; Wan, L.; Liao, Y.; Pang, M.; Xu, Q.; Wang, P.; Wang, B. Continuous Ammonia Electrosynthesis Using Physically Interlocked Bipolar Membrane at 1000 mA cm^{-2}. *Nat. Commun.* **2023**, *14*, 1619.
(32) Xu, Z.; Liao, Y.; Pang, M.; Wan, L.; Xu, Q.; Zhen, Y.; Wang, B. A Chemically Interlocked Bipolar Membrane Achieving Stable Water Dissociation for High Output Ammonia Electrosynthesis. *Energy Environ. Sci.* **2023**, *16* (9), 3815−3824.
(33) Evich, M. G.; Davis, M. J. B.; McCord, J. P.; Acrey, B.; Awkerman, J. A.; Knappe, D. R. U.; Lindstrom, A. B.; Speth, T. F.; Tebes-Stevens, C.; Strynar, M. J.; Wang, Z.; Weber, E. J.; Henderson, W. M.; Washington, J. W. Per- and Polyfluoroalkyl Substances in the Environment. *Science* **2022**, *375*, No. eabg9065.
(34) Hnát, J.; Plevová, M.; Žitka, J.; Paidar, M.; Bouzek, K. Anion-Selective Materials with 1,4-Diazabicyclo[2.2.2]Octane Functional Groups for Advanced Alkaline Water Electrolysis. *Electrochim. Acta* **2017**, *248*, 547−555.
(35) Pagels, M. K.; Adhikari, S.; Walgama, R. C.; Singh, A.; Han, J.; Shin, D.; Bae, C. One-Pot Synthesis of Proton Exchange Membranes from Anion Exchange Membrane Precursors. *ACS Macro Lett.* **2020**, *9* (10), 1489−1493.
(36) Ziv, N.; Dekel, D. R. A Practical Method for Measuring the True Hydroxide Conductivity of Anion Exchange Membranes. *Electrochem. Commun.* **2018**, *88*, 109−113.
(37) Vermaas, D. A.; Wiegman, S.; Nagaki, T.; Smith, W. A. Ion Transport Mechanisms in Bipolar Membranes for (Photo)-Electrochemical Water Splitting. *Sustain Energy Fuels* **2018**, *2* (9), 2006−2015.
(38) Ge, Z.; Shehzad, M. A.; Ge, L.; Zhu, Y.; Wang, H.; Li, G.; Zhang, J.; Ge, X.; Wu, L.; Xu, T. Beneficial Use of a Coordination Complex As the Junction Catalyst in a Bipolar Membrane. *ACS Appl. Energy Mater.* **2020**, *3* (6), 5765−5773.
(39) Tricker, A. W.; Lee, J. K.; Babbe, F.; Shin, J. R.; Weber, A. Z.; Peng, X. Engineering Bipolar Interfaces for Water Electrolysis Using Earth-Abundant Anodes. *ACS Energy Lett.* **2023**, *8* (12), 5275−5280.
(40) Marino, M. G.; Kreuer, K. D. Alkaline Stability of Quaternary Ammonium Cations for Alkaline Fuel Cell Membranes and Ionic Liquids. *ChemSusChem* **2015**, *8* (3), 513−523.
(41) You, W.; Hugar, K. M.; Selhorst, R. C.; Treichel, M.; Peltier, C. R.; Noonan, K. J. T.; Coates, G. W. Degradation of Organic Cations under Alkaline Conditions. *J. Org. Chem.* **2021**, *86* (1), 254−263.
(42) Lindquist, G. A.; Gaitor, J. C.; Thompson, W. L.; Brogden, V.; Noonan, K. J. T.; Boettcher, S. W. Oxidative Instability of Ionomers in Hydroxide-Exchange-Membrane Water Electrolyzers. *Energy Environ. Sci.* **2023**, *16* (10), 4373−4387.
(43) Wang, Z.; Parrondo, J.; Ramani, V. Anion Exchange Membranes Based on Polystyrene-*Block*(ethylene-*ran*-butylene)-*Block*-Polystyrene Triblock Copolymers: Cation Stability and Fuel Cell Performance. *J. Electrochem. Soc.* **2017**, *164* (12), F1216−F1225.
(44) Kwak, M.; Ojha, K.; Shen, M.; Boettcher, S. W. Electrically Insulated Catalyst − Ionomer Anode Interfaces toward Durable Alkaline Membrane Electrolyzers. *ACS Energy Lett.* **2024**, *9* (3), 1025−1034.

https://doi.org/10.1021/acsenergylett.4c01178
ACS Energy Lett. 2024, 9, 2953−2959